PCCP

PAPER

View Article Online
View Journal | View Issue

Cite this: *Phys. Chem. Chem. Phys.*, 2019, **21**, 14195

Photon catalysis of deuterium iodide photodissociation†

Kallie I. Hilsabeck,‡[a] Jana L. Meiser,‡[a] Mahima Sneha,‡[a] N. Balakrishnan [b] and Richard N. Zare *[a]

Received 28th September 2018,
Accepted 26th November 2018

DOI: 10.1039/c8cp06107f

rsc.li/pccp

A catalyst enhances a reaction pathway without itself being consumed or changed. Recently, there has been growing interest in the concept of "photon catalysis" in which nonresonant photons, which are neither absorbed nor scattered, promote reactions. The driving force behind this effect is the interaction between the strong electric field associated with a pulsed, focused laser and the polarizability of the reacting system. In this study, the effect of near-infrared, nonresonant radiation on the photodissociation of deuterium iodide is demonstrated. We use nanosecond pulses rather than time-resolved spectroscopy to investigate the average effect of the electric field on the branching ratio for forming D + I($^2P_{3/2}$) and D + I($^2P_{1/2}$). Changes in the measured D-atom speeds between field-free and strong-field conditions confirm substantial differences in dissociation dynamics. Both the magnitude and direction of change in the branching ratios are dependent upon the photodissociation wavelength. Experiments and theoretical calculations confirm that the mechanism for photon catalysis under these conditions is dynamic Stark shifting of potential energy surfaces rather than electric-field-induced alignment of reagent molecules.

I. Introduction

Chemists strive to achieve control over chemical reactions by manipulating such physical variables as pressure, temperature, solvent polarity, and reagent concentration; however, even thermodynamically favored reactions often resist yielding appreciable amounts of product because the kinetics are too slow. The key to unlocking such reactions is to find a suitable catalyst, a species that enhances the rate of a reaction without itself being used up or changed.

Catalysis is a vast and quickly developing area in chemical research with applications in several fields of science and technology. Standard examples of chemical catalysts include enzymes, organometallic complexes, and metal surfaces. Although very different in structure, each of these substances share a common function: through electric fields, they interface with specific bonds or functional groups within a reacting compound.[1,2] The result of this action is to lower the energy of the transition state for a specific reaction pathway relative to others, thus enhancing its reaction rate. Applying electric forces[3] to reacting molecular systems can be achieved even in the absence of a traditional chemical catalyst, for example, through the application of a focused laser pulse.

Light exists as a propagating wave of electric and magnetic fields. For decades, the interaction of light with matter has been used to induce spectroscopic transitions through the resonant excitation of molecules to rotational, vibrational, and electronic excited states. The effect of nonresonant radiation is often considered to be insignificant and disregarded; however, this assumption is only valid in the limit of a "weak" field.[2] With pulsed lasers, it is possible to achieve electric field strengths that exceed by orders of magnitude the static field strengths supplied by common high-voltage power supplies. For example, an IR laser pulse (1064 nm) of 4 W focused to a beam waist radius of 30 μm and having a duration of 10–11 ns, has a peak intensity of 3.4×10^{12} W cm^{-2} and electric field strength, ε_0, on the order of 5.0×10^7 V cm^{-1}. At these high laser powers, nonresonant radiation, through its electric field, can influence the course of a reaction by interacting with the molecular system's polarizability α to lower an activation barrier directly. Because there is no net consumption of photons in this process, the photons behave as catalysts rather than reactants in a process referred to as photon catalysis, or laser field catalysis as it was first defined by Stolow and coworkers.[1,2,4,5]

To elaborate, consider a simple collinear molecular system, *e.g.*, the photodissociation of a linear molecule. For frequencies much greater than the reciprocal of the laser

[a] *Department of Chemistry, Stanford University, Stanford, CA, 94305, USA. E-mail: rnz@stanford.edu*
[b] *Department of Chemistry and Biochemistry, University of Nevada, Las Vegas, NV, 89154, USA*

† Electronic supplementary information (ESI) available. See DOI: 10.1039/c8cp06107f

‡ These authors contributed equally to this research.

pulse duration, the Hamiltonian can be written in the following way:

$$\bar{H} = H_0 + BJ^2 - \frac{1}{4}\varepsilon_0^2\left[\alpha_\perp + \left(\alpha_\parallel - \alpha_\perp\right)\cos^2\theta\right], \quad (1)$$

where $H_0 + BJ^2$ describes a rotating molecular system in the absence of an external field, ε_0 is the electric field strength, θ is the angle between the electric field and the molecular axis, and $\alpha_\parallel$ and $\alpha_\perp$ represent the polarizabilities of the linear system, parallel and perpendicular to the molecular axis.[6] Please note that possible interaction with a permanent dipole moment averages to zero and therefore is not included. The term in square brackets in this equation clearly outlines two possible effects of a strong, nonresonant electric field on a molecular system:

(1) Stark shift of energy levels – the bracketed terms that are independent of θ result in a Stark shift of the molecule's potential energy surfaces. The distortion of these surfaces may alter adiabatic and/or nonadiabatic dissociation dynamics by impacting the intersection geometry and Landau–Zener hopping probabilities, thereby enhancing or depleting the contribution from the available channels to the total product yield.

(2) Alignment – the term involving $\cos^2\theta$ mixes rotational levels, causing the molecular system to become aligned in the presence of a strong electric field. This behavior is most prevalent for atoms/molecules in the ground rotational state. The effect of alignment on the dissociation dynamics is dependent upon the anisotropy of the dissociation and the polarization of the strong electric field.

Hydrogen halide and dihalide molecules provide model theoretical[7–14] and experimental[15–23] systems for photodissociation reactions involving an excitation from the ground state to an electronically excited potential energy surface. Because they are well-characterized in the literature and exhibit significant polarizability even in the ground state, these simple molecules are also excellent starting points for the experimental demonstration of photon catalysis. To date, the most well-known observation of photon catalysis involved the photodissociation dynamics of IBr, a dihalide molecule. Stolow and coworkers[1] used time-resolved, ultrafast spectroscopy to confirm that application of a strong, nonresonant infrared (IR) field (λ = 800 nm) led to substantial changes in the relative contributions of two competing IBr dissociation channels. This study demonstrated one of the possible effects of strong, nonresonant radiation on a molecular system: dynamic Stark shifting of potential energy surfaces to energetically favor the formation of one product over another. For this system, with nearly purely repulsive excited state surfaces, the nonresonant field did not catalyze the reaction by lowering an energy barrier along any one excited potential surface. Instead, the IR field catalyzed one reaction pathway by enhancing its rate relative to another, without being consumed, through Stark shifting of potential energy surfaces. Another study by Bañares and coworkers[4] demonstrated that the presence of an ultrafast strong laser field gives rise to light induced conical intersections in the CH_3I potentials, leading to a substantial change in the branching ratio of different product channels in the photolysis of this molecule.

It has also been experimentally observed that a second effect, alignment of reagent molecules by a nonresonant laser field, can lead to a change in the contribution of different channels to the overall product yield. Stapelfeldt *et al.*[24] demonstrated control over the ratio between two photodissociation channels of iodine (I_2) through application of a strong, near-IR laser pulse polarized either parallel or perpendicular to the polarization axis of the excitation laser pulse. This result is consistent with the anisotropic nature of the photodissociation: the two major product channels are related adiabatically to two different excited potential energy surfaces that are accessed through either a parallel or perpendicular transition, respectively. Therefore, one of the product channels is favored when the aligning and dissociating laser pulses are polarized in the same direction, and the other channel is favored when the two lasers are polarized perpendicularly to each other. Similar studies involving linear molecules like OCS (Sakai *et al.*[25]), as well as more complex compounds like pyrimidine (Franks *et al.*[26]), also have shown that it is possible to control a molecule's alignment using a strong electric field.

In the work presented here, we studied the impact of the two aforementioned effects of a strong, nonresonant, near-IR field on photodissociation of deuterium iodide (DI). As in the case of IBr, DI exhibits prompt dissociation from nearly purely repulsive surfaces. Two channels arise from the spin–orbit interactions in the iodine atom.[7–10,15–20] The spin–orbit excited state of the I atom ($^2P_{1/2}$) is higher in energy than the ground state I atom ($^2P_{3/2}$) by 0.94 eV. Therefore, the dissociation channel D + I($^2P_{3/2}$), where the I is in its ground state, has higher kinetic energy disposed in the corresponding D atom and is known as the fast channel. The slow channel corresponds to the spin–orbit excited state of iodine, I($^2P/_{1/2}$), which hereafter will be denoted by I*. By the necessity that total energy be conserved, this channel has slower-moving D atoms. The extent to which each channel is populated depends upon the potential energy curve to which the molecule is initially excited (*i.e.*, the energy of the exciting photon), and the probability for nonadiabatic transitions within the Franck–Condon region (Fig. 1). The ratio of the respective reaction cross sections, σ, of the slow channel to the fast channel is referred to as the branching ratio, $\sigma[I^*]/\sigma[I]$. The wavelength dependence of the branching ratio in the absence of a strong electric field has previously been characterized, and is observed to peak approximately at 250 nm.[15] By monitoring changes in the branching ratio with application of strong, nonresonant radiation, experimental results provided insight into the photon-catalyzed process.

Simple theoretical calculations that model the effect of dynamic Stark shifting on the branching ratio were performed to complement and qualitatively support experimental results. The photodissociation dynamics were treated using the time-dependent wave packet formalism. Details of the field-free dynamics are given in prior works.[7–9] Although the photodissociation dynamics of HI in the presence of two-color, intense laser pulses has been reported previously,[27] the effect

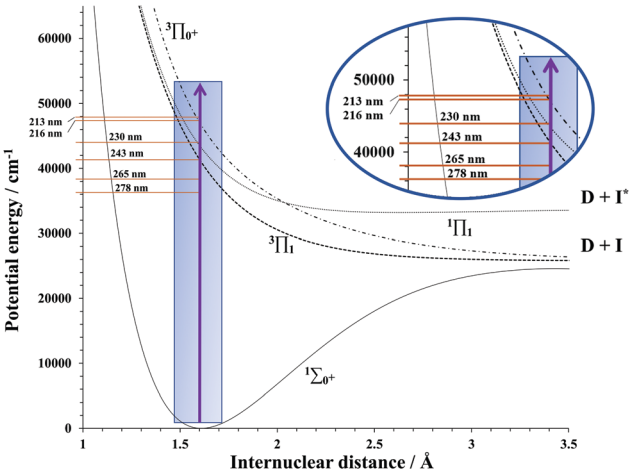

Fig. 1 Potential energy curves for the ground and low-lying excited electronic states of DI involved in one-photon dissociation. The parts of the potential that were sampled at each experimental excitation wavelength, within the Franck–Condon region, are illustrated schematically.

of a pulsed, nonresonant electric field on the dissociation dynamics and the I*/I branching ratio has not been theoretically explored. Below, we provide a brief description of the theoretical approach, following the methods given in ref. 9 and 27.

The time-dependent Schrödinger equation was solved to describe the photodissociation dynamics of DI in the A band. Five electronic states were considered in the study: $X^1\Sigma^+$, $^3\Pi_1$, $^1\Pi_1$, $^3\Pi_{0+}$, and $t^3\Sigma_1^+$, denoted $V_i(R)$, i = 1–5. The Schrödinger equation may be written as

$$i\hbar\frac{\partial\boldsymbol{\Psi}(R,t)}{\partial t}=\left[-\frac{\hbar^2}{2m}\boldsymbol{I}\frac{\mathrm{d}^2}{\mathrm{d}R^2}+\boldsymbol{U}(R)\right]\boldsymbol{\Psi}(R,t), \qquad (2)$$

where $\boldsymbol{\Psi}$ is a column vector of wave functions with components ψ_i, i = 1–5, for the five electronic states, $\boldsymbol{I}$ is a 5 × 5 identity matrix, and $\boldsymbol{U}(R)$ is a 5 × 5 potential energy matrix with the diagonal elements,

$$U_i(R)=V_i(R)-\frac{1}{4}\alpha_i(R)\varepsilon_0(t)^2. \qquad (3)$$

The second term of eqn (3) denotes the Stark-shift of the potential curves due to the electric field. Rotational effects were ignored in our calculations, and the polarizability term was approximated by its parallel component, with values taken from Maroulis[28] for the $X^1\Sigma^+$ state. The anisotropy of the polarizability is quite small for the ground state of HI, $\Delta\alpha = \alpha_\parallel - \alpha_\perp$ = 2.94 a.u., compared to the parallel component, $\alpha_\parallel$ = 37.98 a.u., at the equilibrium internuclear separation. The Stark shift was applied only to the excited state potential curves ($V_i(R)$, i = 2–5).

Alignment, the second possible effect of a nonresonant field, is also investigated experimentally. The studies on HI photodissociation by Langford *et al.*,[15] and DI dissociation by Heck and Chandler[29] show that independent of wavelength of excitation, the fast and slow channels for both HI and DI result predominantly from adiabatic perpendicular and parallel transitions, respectively. Therefore, changing the relative polarizations of the near-IR pulse and exciting pulses allows for the deconvolution of the effects of Stark shifting and alignment on reaction outcome. This study is further distinguished from previous work because nanosecond pulses are employed to supply the field, which are much longer than the timescale of the reaction. This presents an opportunity to determine the more general effect that a nonresonant electric field had on modifying total reaction yield, rather than doing a time-resolved study. It is also more conducive to future extension of the effect beyond unimolecular reactions, *e.g.*, to bimolecular reactions such as DI + D → $D_2(v', j')$ + I.[30,31]

II. Methods

Experimental details

A detailed description of the experimental setup has been provided in previous publications.[32] For this set of experiments, a mixture of 5% DI (D 98%, Cambridge Isotopes Laboratories, Inc.) in an inert carrier gas (Ar, He) was expanded supersonically into a vacuum chamber through a pulsed valve (General Valve, Series 9) at a stagnation pressure of 10–15 psi. We observed no significant differences in the branching ratios using different carrier gases. The molecular beam was collimated through a 2 mm skimmer and intersected orthogonally by focused photolysis and photoionization (probe) lasers, as well as the IR laser (1064 nm) that supplied the strong electric field. Resulting positively charged D^+ ions were accelerated through a Wiley–McLaren time-of-flight (TOF) mass spectrometer and collected on a position-sensitive delay-line detector. Time and position information were used to extract lab-frame speed distributions for the product D^+ ions. The branching ratios were calculated by integrating the relative areas under the slow and fast channel peaks in the speed distributions.

DI photodissociation was carried out at six wavelengths in the A-band between 213 and 278 nm, both with and without the strong electric field supplied by the near-IR laser. Under each set of conditions, three to five reproducible data sets, averaging over 3000–4000 ions, were collected. For each experiment, the photolysis laser power was maintained at approximately 10–20 μJ. The D-atom product was ionized using (2 + 1) resonance enhanced multiphoton ionization (REMPI) *via* the 2s–1s transition at approximately 243 nm. Under the application of the strong electric field, the REMPI line was red-shifted 10–20 pm to account for the observed Stark shift of the D-atom signal. A probe laser power of 5 μJ was sufficient for this experimental setup. The average power peak intensity of the IR laser was maintained between 3.4 × 10^{12} W cm^{-2} and 5.1 × 10^{12} W cm^{-2}, which, when focused with a lens of f = 35 cm, corresponds to an electric field strength of approximately 5.1 × 10^7 V cm^{-1} to 6.3 × 10^7 V cm^{-1} in the interaction volume. Low powers of the UV lasers ensured that the strong electric field was solely produced by the IR laser. A detailed description of the method of background subtraction is provided in the ESI† (Fig. S1).

Two techniques were used for D-atom detection. For excitation wavelengths of 213 nm, 216 nm, 243 nm, and 278 nm, the

Doppler-free technique was implemented. Two counterpropagating UV lasers were overlapped spatially and temporally, and their wavelengths were chosen such that combined they achieved resonance with the (2 + 1)-REMPI line at 243 nm. The dissociation laser was set at higher power so that it solely photolyzed the DI molecule. Minimal photolysis contamination from the other UV laser was subtracted as background. Because both lasers contributed to the probe step and were traveling in opposite directions toward the interaction region, D atoms were ionized regardless of their speed with respect to the laser propagation direction. This condition strongly increased the signal without impacting the amount of background in our experiments. Furthermore, as the Doppler-free technique removed the requirement to perform a scan over the Doppler range, it reduced inconsistencies arising from power and overlap fluctuations of the lasers throughout data collection and produced speed distributions with a more Gaussian shape.

For 265 nm and 230 nm excitation, a traditional pump–probe setup was used. DI molecules were first dissociated by the pump laser and, after a short time delay of 3 ns, the resulting D-atom product was ionized using (2 + 1)-REMPI *via* the 2s–1s transition at approximately 243 nm. The probe laser wavelength was scanned over the Doppler range. This detection technique was chosen for these two wavelengths because the complementary UV wavelength required to fulfill the Doppler-free condition either produced strongly overlapping peaks in the speed distribution (265 nm, Fig. S2, ESI†) or caused an overwhelming amount of multiphoton background with the IR (230 nm).

The ultraviolet laser light of appropriate wavelengths for the photolysis and photoionization processes was attained in two ways: frequency tripling the output of a dye laser (Lambda Physik, LPD 3000) pumped by the second harmonic of an Nd:YAG^{3+} laser (Spectra Physics, GCR Series), or frequency doubling the output of a dye laser (Lambda Physik, LPD 3000) pumped by the third harmonic of an Nd:YAG^{3+} laser (Quanta-Ray, DCR-3). The strong electric field was supplied by the fundamental of a third Nd:YAG^{3+} laser (Spectra Physics, GCR Series) at 1064 nm. All frequency mixing was achieved using BBO crystals.

Computational details

Theoretical calculations correspond to a pulse width of τ = 500 fs. Although we used a much longer IR pulse for our experiments, the probability for excitation and dissociation from each excited potential surface reached a steady state within about 50 fs, by which time the electric field also had reached 97% of its peak value (Fig. S3, ESI†). Therefore, this approximation is reasonable for comparison with our experimental results.

In the absence of any literature results on the polarizabilities of HI for the various excited electronic states considered here, we have approximated the excited state polarizabilities, $\alpha_i(R) = \alpha_1(R) \times f(i)$, i = 2–5, where $\alpha_1(R)$ is the polarizability of the ground state and $f(i)$, i = 2–5 are scaling factors for the excited state polarizabilities. We have taken wide latitude in choosing the scaling factors to explore any unusually large effect induced by the electric field. Different sets of calculations were performed with different values of the scaling parameters to examine the sensitivity of results to the shift in the excited state potentials induced by the electric field. Five different sets of calculations were performed for a given laser intensity with the excited state polarizabilities varied by a factor of 1.2 to a factor of 15. They are listed below as Shift 1 through Shift 5:

Shift1: $f(2) = 1.2, f(3) = 1.3, f(4) = 1.5, f(5) = 1.5$
Shift2: $f(2) = 2.0, f(3) = 2.5, f(4) = 3.0, f(5) = 3.0$
Shift3: $f(2) = 3.0, f(3) = 3.5, f(4) = 4.0, f(5) = 4.0$
Shift4: $f(2) = 4.0, f(3) = 4.5, f(4) = 5.0, f(5) = 5.0$
Shift5: $f(2) = 10.0, f(3) = 11.0, f(4) = 15.0, f(5) = 15.0$

In each case, $f(4)$ and $f(5)$ were assumed to be the same, as excited state 5 does not contribute appreciably to the one-photon dissociation process in the wavelength range reported here. Although this choice of scaling factors is rather arbitrary, large variations in excited state polarizabilities with factors from 2–6 have been reported for diatomic molecules such as LiH and NaH.[33] Preliminary *ab initio* calculations without the inclusion of spin–orbit coupling also suggest a factor of 2 or higher values for the excited state polarizabilities with strong anisotropic components. Table S1 (ESI†) presents details of this calculation in the ESI.†

The off-diagonal elements $U_{1i}(R) = U_{i1}(R)$, i = 2–5 of $\boldsymbol{U}(R)$ denote the field-induced couplings, which in the dipole approximation are given by $U_{1i}(R) = -\mu_{1,i}(R)\varepsilon_0(t)\cos(\omega t)$, i = 2–5 where $\mu_{1,i}(R)$ are the R-dependent transition dipole moments between the ground state and the excited electronic states, i = 2–5. The electric field is defined as $\varepsilon_0(t) = \varepsilon_0 g(t)$, where ε_0 is the peak field strength, and the envelope function $g(t)$ is taken to be a Gaussian centered at $t = 0$, $g(t) = \exp[-4\ln(2)t^2/\tau^2]$ with full-width τ at half-maximum.

The excited-state potential curves and transition dipole moments are taken from Camden *et al.*,[34] which provide experimentally calibrated parameters. We used parameters corresponding to model 1 in Table 3 of Camden *et al.*[34] The branching ratio is very sensitive to the slope of the excited state potential curves in the Franck–Condon region, and the potential curves and dipole moment functions of model 1 yield better agreement with experiment than the *ab initio* potential curves and transition dipole moments of Alekseyev *et al.*[35] However, Alekseyev *et al.*[36] have also argued that a slight upward shift of approximately 500 cm^{-1} of the *ab initio* computed excited triplet potential curves and a 5% increase in the $(^1\Pi_1, ^3\Pi_1) \leftarrow X$ transition dipole moments yield results in close agreement with experiment, an analysis that also favors model 1 parameters. For the ground $X^1\Sigma^+$ state, we used the potential energy curve of Coxon and Hajigeorgiou[37] in the short-range and merged it smoothly with the *ab initio* potential of Alekseyev *et al.*[35] for $R > 6.3$ bohr. We have also included the spin-rotation coupling between the $^1\Pi_1$ and $^3\Pi_{0+}$ states as an off-diagonal matrix element $U_{34}(R) = U_{43}(R)$, but this has a negligible effect on the branching ratio as found for field-free dynamics in ref. 9. Although we have included the $t^3\Sigma_1^+$ electronic state correlating with I* channel in our calculations,

its effect is not important and it does not contribute to I* channel at the excitation wavelengths considered in this work.

The Schrödinger equation was solved using the split-operator method[38] with appropriate absorbing boundary conditions.[39] The wave packet was initialized as $\psi_1(R,t = 0) = \phi_{v=0,j=0}(R)$, $\psi_i(R,t = 0) = 0$, $i = 2$–5, where $\phi_{v=0,j=0}(R)$ is the rovibrational ground state wave function of the $X^1\Sigma^+$ state. A radial grid of 512 points in the range $R = 2$–20 a.u. was used to discretize the wave packet. Diagonalization of the potential matrix at each time step of the propagation yields a set of adiabatic ''light-shifted'' potential curves. See ref. 9 and 39 for more details.

III. Results & discussions

Deuterium iodide was photodissociated under field-free conditions and in the presence of the strong electric AC field supplied by a nonresonant, near-IR laser pulse at 1064 nm. Fig. 2a–f present the measured D-atom speed distributions for six excitation wavelengths spanning the A band: Fig. 2a at 213 nm, Fig. 2b at 216 nm, Fig. 2c at 230 nm, Fig. 2d at 265 nm, Fig. 2e at 243 nm, and Fig. 2f at 278 nm. Table S2 (ESI†) lists the fast and slow D-atom speeds for the excitation wavelengths used in this study. For these sets of experiments, the excitation laser pulse was polarized vertically, and the IR laser pulse was polarized horizontally.

The experimental branching ratios under field-free conditions were in reasonable agreement with previously published values.[15] Upon application of a strong AC field that encompassed the entire photodissociation process, we observed significant changes in the branching ratios to one standard deviation. These experimental findings provide clear evidence of the measurable effect of a nonresonant IR field on the photodissociation dynamics of DI. Furthermore, because IR photons were neither absorbed nor changed during this process, they acted as catalysts to selectively lower activation barriers for one pathway relative to another.

Both the magnitude and direction of this change were dependent upon the excitation energy. At 213 nm and 216 nm (Fig. 2a and b), the branching ratio decreased by 23% and 14%, respectively, under strong field conditions, suggesting that the fast product channel was enhanced relative to the slow channel by the application of the IR field in this wavelength range. Conversely, at 230 nm and 265 nm (Fig. 2c and d), the branching ratio increased significantly by 36% and 39%, respectively, which indicates a relative increase in the slow channel contribution with application of the IR field. No measurable change in the branching ratio was perceived for photodissociation at 243 nm or 278 nm (Fig. 2e and f). Higher intensity IR experiments were performed for excitation at 216 nm and 243 nm. As is evident from Fig. 2b and e, this increase in electric field strength was not sufficient to produce a measurable change from the branching ratio at the lower IR power. Table 1 summarizes the results.

A third peak was observed in the case of Fig. 2a, b and f. As mentioned previously, the Doppler-free probing technique used for these excitation wavelengths involved two counter-propagating lasers that can each contribute to photolysis. These additional peaks were the result of a small amount of DI photolysis by the other UV laser, which could not be fully accounted for in the background subtraction. However, as these peaks were well-separated from the slow and fast channels resulting from the excitation wavelength, they did not interfere with branching ratio determination. Similarly, small shoulders on the leading edges of the slow and fast channel peaks in Fig. 2c corresponded to 243 nm dissociation by the probe laser. Shoulders were not included in the area that was integrated for the branching ratio calculations; however, inclusion of the shoulder for both the slow and fast channel peaks did not cause the branching ratio to fall outside of the currently reported uncertainty because the branching ratio at 243 nm was approximately equal to 1 for both the field-free and IR-field cases.

It should also be noted that the two excitation wavelengths for which an increase in the slow channel were observed, 230 nm and 265 nm, were also the two wavelengths that employed the pump–probe approach. To confirm that this result was not caused by a systematic bias introduced by the detection technique, the experiments at 243 nm excitation were repeated using a one-laser, pump–probe approach. With both the Doppler-free and pump–probe techniques, the same result was observed: no change in branching ratio was detected with application of the strong field (Fig. S4a and b, ESI†). Furthermore, the experiments at 230 nm were repeated with a 0 ns delay instead of 3 ns to ensure that the enhancement in the slow channel was not artificially created because of the faster moving atoms escaping the interaction volume before ionization. Measured speed distributions and branching ratios were not influenced by a time delay of this magnitude, under either field-free or IR-field conditions. Collectively, these results indicate that no systematic bias existed in our detection setup.

Degree of alignment

Because the slow and fast channels correspond predominately to parallel and perpendicular transitions, respectively, alignment of reactant molecules with the electric field should favor one channel over the other, resulting in products with different branching ratios. In the experiments presented to this point, the excitation laser and IR laser were polarized perpendicularly to one another, and any significant alignment would have favored the formation of faster-moving D atoms. To evaluate the extent of alignment in the beam, we repeated the experiments at an excitation wavelength of 278 nm with a vertical polarization of the IR beam, parallel to the polarization of the excitation laser pulse (Fig. 3).

As Fig. 3 and Table 1 indicate, the branching ratio in the presence of the strong field was independent of the polarization of the IR laser pulse relative to that of the excitation laser pulse at an excitation wavelength of 278 nm. Calculations predict that most of the alignment should occur for molecules in the ground rotational state, $J = 0$.[40] To determine the percentage of molecules present in the ground rotational state,

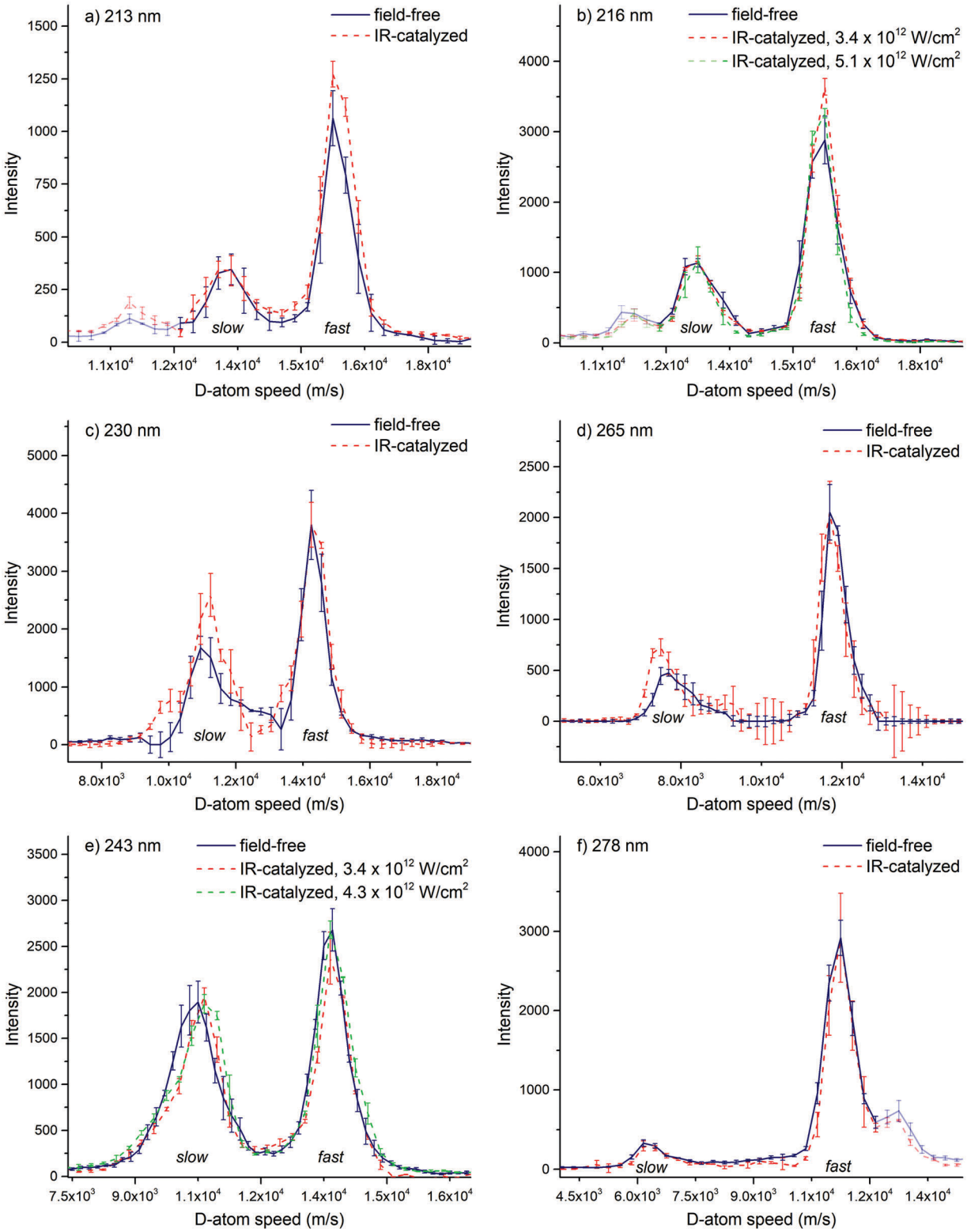

Fig. 2 D-Atom speed distributions for the photodissociation of DI at a series of excitation wavelengths: (a) 213 nm, (b) 216 nm, (c) 230 nm, (d) 265 nm, (e) 243 nm, and (f) 278 nm. The blue lines represent data collected in the absence of a strong electric field (field-free), and the red dashed lines represent data collected at an IR peak intensity of 3.4×10^{12} W cm^{-2} ($\varepsilon_0 = 5.1 \times 10^7$ V cm^{-1}, IR-catalyzed). The green dashed lines in (b) and (e) are for experiments performed at higher IR peak intensities of 4.3×10^{12} W cm^{-2} and 5.1×10^{12} W cm^{-2}, respectively ($\varepsilon_0 = 5.8 \times 10^7$ V cm^{-1}, and 6.3×10^7 V cm^{-1}). Error bars denote one standard deviation over 3–5 experimental data sets. A third peak is observed in the case of a, b, and f, here marked in a lighter shade for clarity, which originates from photolysis by the complementary Doppler-free probe laser. The shoulders on the leading edges of the fast and slow channel peaks in c are also consistent with 243 nm dissociation by the probe laser.

Table 1 Experimentally measured branching ratios for the photodissociation of DI in the presence and absence of a strong, nonresonant IR field. Uncertainties represent one standard deviation over 3–5 experimental data sets

Excitation wavelength (nm)	IR field-free branching ratio	Branching ratio for IR peak intensity = 3.4×10^{12} W cm^{-2} ($\varepsilon_0 = 5.1 \times 10^7$ V cm^{-1})[a]
213	0.52 ± 0.02	0.40 ± 0.02
216	0.50 ± 0.02	0.43 ± 0.02
230	0.67 ± 0.08	0.91 ± 0.08
243	1.01 ± 0.04	1.00 ± 0.03
265	0.31 ± 0.04	0.43 ± 0.02
278 (H)[b]	0.13 ± 0.01	0.12 ± 0.01
278 (V)[b]	0.13 ± 0.01	0.12 ± 0.01

[a] For 243 nm and 216 nm excitation, IR experiments were also performed at $\varepsilon_0 = 5.8 \times 10^7$ V cm^{-1} and 6.3×10^7 V cm^{-1}, but there were no measurable changes from the branching ratio at 5.1×10^7 V cm^{-1}. [b] For 278 nm excitation, data were collected with the IR laser polarized horizontally (H) and vertically (V).

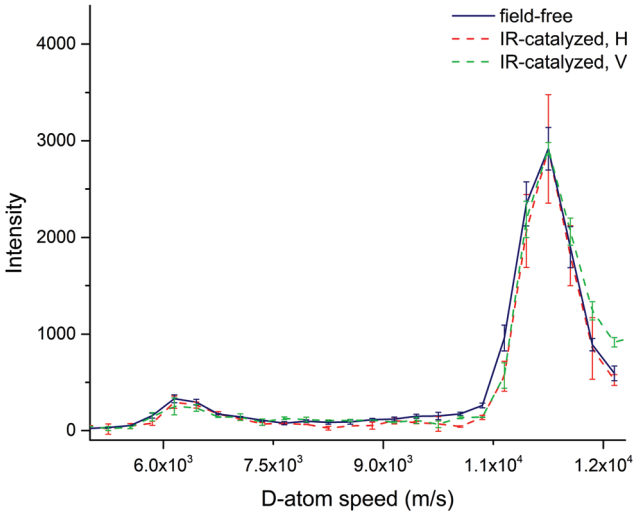

Fig. 3 D-Atom speed distributions for the photodissociation of DI at 278 nm in the absence (blue line) and presence of vertically polarized (red dashed line) and horizontally polarized (green dashed line) IR field. Error bars denote one standard deviation over 3–5 experimental data sets.

the rotational distribution of DI in the molecular beam was measured. A large iodide ion background signal at the desired wavelengths precluded a quantitative measurement; however, qualitatively it was confirmed that there were roughly five times more molecules in the $J = 1$ level than in the $J = 0$ level, and that a discernable DI signal existed for rotational levels up to $J = 10$. Fig. S5 in the ESI† displays an approximation for the rotational distribution of DI in our molecular beam. As the majority of the DI molecules in the molecular beam have non-zero rotational energy ($J \neq 0$), this result is consistent with no detectable alignment by an external electric field at an excitation wavelength of 278 nm (Fig. 3). This result is general, as alignment is not expected to be wavelength-dependent. The negligible impact of alignment under these experimental conditions suggests that the observed photon catalysis effect arose primarily because of the dynamic Stark shifting of potential energy surfaces, rather than electric-field-induced alignment.

Dynamic Stark-shifting of potential surfaces

Theoretical calculations were performed to make a qualitative prediction about how the dynamic Stark shifting of potential energy surfaces is expected to impact the relative contributions of the slow and fast channels to the dissociation of DI. Excited state polarizabilities were scaled up from the ground state over a range of scaling factors, as described above, to give an estimate of the expected Stark shifts. At an electric field strength of 5.1×10^7 V cm^{-1}, shifts 1–4, corresponding to different scaling factors, yielded comparable results. Conversely, shift 5 displayed an entirely different behavior that suggests that the scaled polarizabilities used were unrealistically large. This result is reflected in the shifted potential energy curves and branching ratios presented in Fig. 4 and 5. In moving forward with the discussion, we take shift 2 as an acceptable approximation for the excited state polarizabilities.

Comparison of the experimental and theoretical data, presented in Fig. 5, clearly shows that the theory cannot quantitatively describe this system or the effect of the nonresonant IR field on its dynamics. However, theoretical calculations do provide qualitative insight into the photon-catalyzed process. The predicted effect of the nonresonant field is to shift the excited potentials to lower energies (Fig. 4), leading to a change in the relative absorption cross sections and a shift in the branching ratio curve to higher wavelengths (Fig. 5).

Observed changes in the branching ratio with application of the IR field are in reasonable qualitative agreement with theoretical calculations for five of the six excitation wavelengths. The smallest changes are predicted for the least sloped regions of the branching ratio curve, which occur at the central peak and edges of the absorption range. This is consistent with the experimental observation of no significant change to the branching ratios at 243 nm and 278 nm. Conversely, the most substantial changes in the branching ratio are expected for the most sloped regions of the curve – experimentally, this corresponds to excitation wavelengths of 213 nm, 216 nm, 230 nm, and 265 nm. Because application of the strong, nonresonant field led to a red-shifting of the branching ratio curve, theory and experiment agreed to a decrease in the branching ratio at 213 nm and 216 nm, and an increase in that ratio at 265 nm. The branching ratio increase that is observed experimentally at 265 nm is notably larger than the theory predicts for shift 2 and smaller than it predicts for shift 5, indicating that actual polarizabilities of the excited states may lie somewhere between the values used for the calculations of shifts 2 and 5.

The branching ratio at 230 nm increased considerably with application of the IR field. The relative enhancement of the slow channel at this photon energy disagrees with our theory and is quite striking compared to the behavior at other wavelengths; however, the observation is not necessarily unexpected. Experimental results at other wavelengths can be understood in terms of a change in the relative probabilities for dissociation through two adiabatic product channels. These observations are

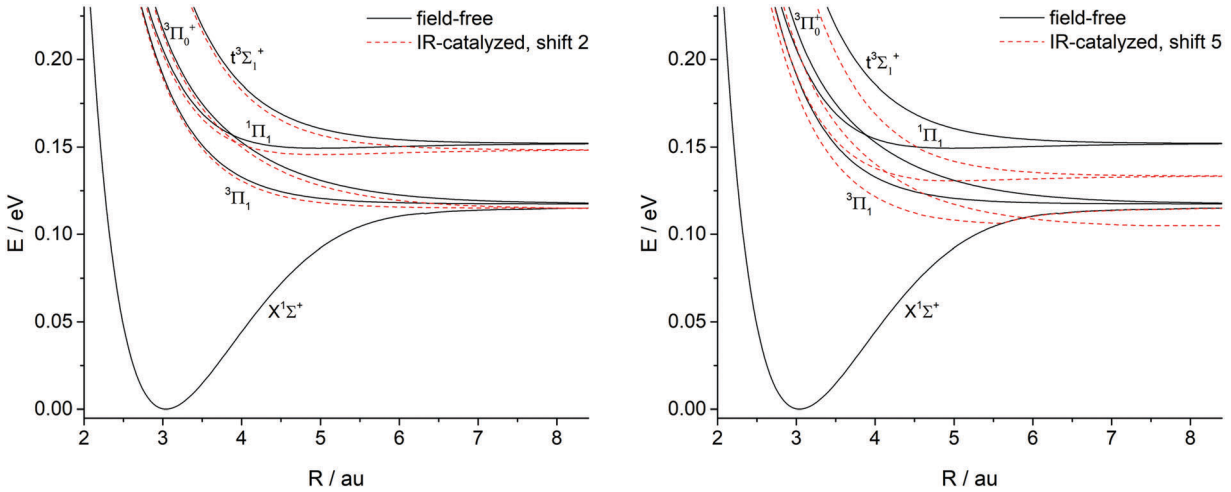

Fig. 4 Potential energy curves for the one-photon dissociation of DI under field-free (black, solid) and IR-catalyzed (red, dashed) conditions using the polarizabilities of (a) shift 2 and (b) shift 5. The electric field strength for these calculations was 5.1×10^7 V cm^{-1}.

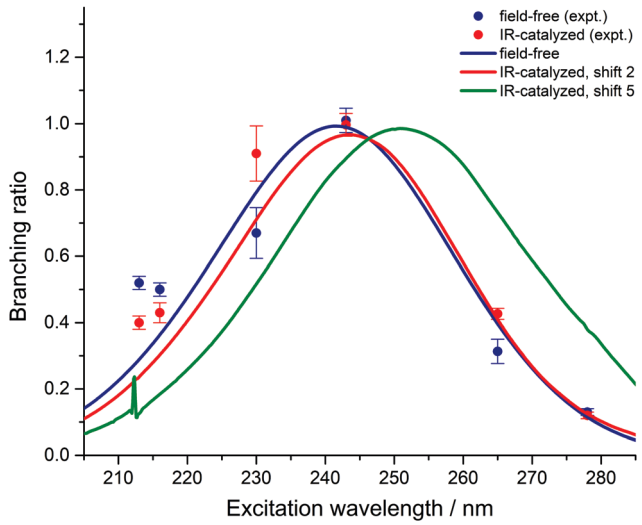

Fig. 5 Experimentally and theoretically determined branching ratios for the photolysis of DI, both in the presence (red and green) and absence (blue) of the strong IR field at 5.1×10^7 V cm^{-1}. Results of calculations for shifts 2 (red) and 5 (green) are displayed. Error bars denote one standard deviation over 3–5 experimental data sets.

qualitatively corroborated by our theoretical model, which adequately describes how the cross-sections for excitation to and dissociation from a single electronic state (*i.e.*, adiabatic transitions) are changed in the presence of a strong field. However, although previous studies report a predominately adiabatic picture of DI's dissociation dynamics, they also suggest a 7% contribution of nonadiabatic channels to the I* product in the range of excitation wavelengths from 227–278 nm.[15,29] The argument in these studies for the major possible source of nonadiabatic behavior is coupling between $^1\Pi_1$ and $^3\Pi_{0+}$ in the Franck–Condon region. After an initial perpendicular excitation to the $^1\Pi_1$ state, the HI/DI molecule dissociates on the $^3\Pi_{0+}$ state, forming the I* product.

We propose that, by changing the position of the avoided crossing between $^3\Pi_{0+}$ and $^1\Pi_1$, the strong field influenced the nonadiabatic dynamics and contributed to the increase in the I* product channel which was observed at 230 nm excitation. Previous experimental observations support this hypothesis. In the ultrafast study of photon-catalyzed IBr photodissociation, Albert Stolow and coworkers[1,2] observed the greatest influence of the strong nonresonant field (*i.e.*, the maximum change in the branching ratio) when the nonresonant pulse arrived as the wavepacket traversed a crossing. A 30% increase in Br* production resulted at this intersection. If the crossing in DI was induced near 230 nm excitation by the strong electric field, a sensitive response to the excitation energy around the crossing is expected: for excitation above or below the crossing, the molecule's hopping probability is not measurably affected, and

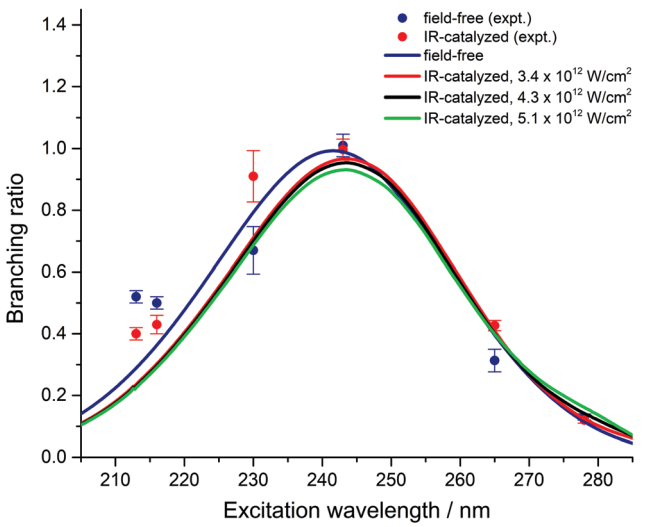

Fig. 6 Theoretically calculated branching ratio curves for the dissociation of DI under field-free conditions (black) and in the presence of a nonresonant IR field at 5.1×10^7 V cm^{-1} (red, 3.4×10^{12} W cm^{-2}), 5.8×10^7 V cm^{-1} (blue, 4.3×10^{12} W cm^{-2}), and 6.3×10^7 V cm^{-1} (green, 5.1×10^{12} W cm^{-2}). Error bars denote one standard deviation over 3–5 experimental data sets.

nonadiabaticity does not play a large role in the dissociation dynamics. These dynamics could not be accurately modeled by our level of theory. How the location of the crossings and coupling strengths vary as a function of the applied field is an interesting issue that clearly warrants more theoretical studies, but is beyond the scope of the present work.

Fig. 6 presents a comparison of the theoretical branching ratio curves for each of the three electric field strengths used in our experiments: 5.1×10^7 V cm^{-1}, 5.8×10^7 V cm^{-1}, and 6.3×10^7 V cm^{-1}. Scaling factors for shift 2 were used for the results presented here. Consistent with experimental measurements, these calculations suggest no significant changes to the branching ratios with an increase of field strength of this magnitude.

IV. Conclusions

In this study, DI was photodissociated at six excitation wavelengths between 213–278 nm in the presence of a nonresonant IR field (1064 nm). The use of nanosecond pulses allowed for determination of the average effect of the strong, nonresonant radiation on overall reaction yield. Changes in the measured branching ratios between field-free and strong field conditions confirm significant differences in dissociation dynamics. Because IR photons enhanced select dissociative pathways relative to others and were not consumed during the reaction, they behaved as catalysts in this process. Experiments and theoretical calculations confirmed that the mechanism for photon catalysis under these conditions was dynamic Stark shifting of potential energy surfaces rather than electric-field-induced alignment of reagent molecules.

Both the magnitude and direction of change in the branching ratios were dependent upon the excitation energy: branching ratios decreased at 213 and 216 nm by 23% and 14%, respectively, increased at 230 and 265 nm by 36% and 39%, and did not change significantly at 243 and 278 nm. Theoretical calculations predict a lowering in energy of excited state potentials, leading to a change in the relative absorption cross sections and a shift in the branching ratio curve toward higher wavelengths. Experiment and theory are in fair qualitative agreement for each excitation wavelength, with the exception of 230 nm. We suggest that the IR field increases nonadiabatic behavior at this photon energy that is not modelled by the level of theory employed, and further investigation is required.

Small changes in the magnitude of the IR field, between 5.1×10^7 V cm^{-1} and 6.3×10^7 V cm^{-1}, did not lead to observable changes in dissociation dynamics. Theory provided confirmation that the relative contributions of the two different channels was much more dependent upon the polarizabilities of the excited states than on small changes in the electric field strength. Future experiments could be completed at significantly higher electric field strengths to characterize the electric field strength dependence on the dynamics of this photon-catalyzed process. Nevertheless, the present study provides clear evidence of the effects of photon catalysis on the photodissociation dynamics of DI.

The dynamic Stark shift impacts all polarizable molecules, suggesting broad chemical applicability. Extension of photon catalysis studies to include bimolecular reactions, reactions involving polyatomic molecules, and reactions in condensed phases may build understanding of its potential for applicability beyond fundamental scientific research.

Conflicts of interest

There are no conflicts to declare.

Acknowledgements

This material is based upon work supported by the National Science Foundation under Grant No. 1464640 and 1806334. K. H., J. M., and M. S. are grateful to Dr Bretislav Friedrich, Fritz-Haber Institute, Berlin, Germany for useful discussions. N. B. is grateful to Keith Lawler for his assistance with computations of excited state polarizabilities of HI presented in the ESI.†

References

1 B. J. Sussman, D. Townsend, M. Y. Ivanov and A. Stolow, *Science*, 2006, **314**, 278–281.
2 A. Stolow, *Nat. Chem.*, 2014, **6**, 759–760.
3 S. D. Fried, S. Bagchi and S. G. Boxer, *Science*, 2014, **346**, 1510.
4 M. Corrales, J. González-Vázquez, G. Balerdi, I. Solá, R. De Nalda and L. Bañares, *Nat. Chem.*, 2014, **6**, 785–790.
5 J. González-Vázquez, I. R. Sola, J. Santamaria and V. S. Malinovsky, *J. Phys. Chem. A*, 2007, **111**, 2670–2678.
6 B. Friedrich and D. Herschbach, *Phys. Rev. Lett.*, 1995, **74**, 4623.
7 A. Brown, *J. Chem. Phys.*, 2005, **122**, 084301.
8 D. N. Jodoin and A. Brown, *J. Chem. Phys.*, 2005, **123**, 054301.
9 N. Balakrishnan, A. Alekseyev and R. Buenker, *Chem. Phys. Lett.*, 2001, **341**, 594–600.
10 I. Levy and M. Shapiro, *J. Chem. Phys.*, 1988, **89**, 2900–2908.
11 G. Péoux, M. Monnerville, T. Duhoo and B. Pouilly, *J. Chem. Phys.*, 1997, **107**, 70–82.
12 A. G. Smolin, O. S. Vasyutinskii, G. G. Balint-Kurti and A. Brown, *J. Phys. Chem. A*, 2006, **110**, 5371–5378.
13 D. Zhang, *J. Math. Chem.*, 2010, **47**, 29–40.
14 M. H. Alexander, B. Pouilly and T. Duhoo, *J. Chem. Phys.*, 1993, **99**, 1752–1764.
15 S. R. Langford, P. M. Regan, A. J. Orr-Ewing and M. N. Ashfold, *Chem. Phys.*, 1998, **231**, 245–260.
16 F. Wang, I.-C. Lu, K. Yuan, Y. Cheng, M. Wu, D. H. Parker and X. Yang, *Chem. Phys. Lett.*, 2007, **449**, 18–22.
17 P. M. Regan, S. R. Langford, A. J. Orr-Ewing and M. N. Ashfold, *J. Chem. Phys.*, 1999, **110**, 281–288.
18 R. D. Clear, S. J. Riley and K. R. Wilson, *J. Chem. Phys.*, 1975, **63**, 1340–1347.
19 B. Huebert and R. Martin, *J. Phys. Chem.*, 1968, **72**, 3046–3048.

20 Z. Xu, B. Koplitz and C. Wittig, *J. Phys. Chem.*, 1988, **92**, 5518–5523.
21 Z. Xu, B. Koplitz and C. Wittig, *J. Chem. Phys.*, 1987, **87**, 1062–1069.
22 Y. Matsumi, K. Tonokura, M. Kawasaki and T. Ibuki, *J. Chem. Phys.*, 1990, **93**, 7981–7985.
23 T. Kinugawa and T. Arikawa, *J. Chem. Phys.*, 1992, **96**, 4801–4804.
24 J. J. Larsen, H. Sakai, C. Safvan, I. Wendt-Larsen and H. Stapelfeldt, *J. Chem. Phys.*, 1999, **111**, 7774–7781.
25 H. Sakai, S. Minemoto, H. Nanjo, H. Tanji and T. Suzuki, *Phys. Rev. Lett.*, 2003, **90**, 083001.
26 K. J. Franks, H. Li and W. Kong, *J. Chem. Phys.*, 1999, **110**, 11779–11788.
27 S.-M. Wang, K.-J. Yuan, Y.-Y. Niu, Y.-C. Han and S.-L. Cong, *Phys. Rev. A: At., Mol., Opt. Phys.*, 2006, **74**, 043406.
28 G. Maroulis, *Chem. Phys. Lett.*, 2000, **318**, 181–189.
29 A. J. R. Heck and D. W. Chandler, *Annu. Rev. Phys. Chem.*, 1995, **46**, 335–372.
30 J. Zhang, J. Jankunas, N. C.-M. Bartlett, N. T. Goldberg and R. N. Zare, *J. Chem. Phys.*, 2010, **132**, 084301.
31 M. A. Buntine, D. P. Baldwin, R. N. Zare and D. W. Chandler, *J. Chem. Phys.*, 1991, **94**, 4672–4675.
32 K. Koszinowski, N. T. Goldberg, A. E. Pomerantz and R. N. Zare, *J. Chem. Phys.*, 2006, **125**, 133503.
33 M. Mérawa, D. Bégué and A. Dargelos, *J. Phys. Chem. A*, 2003, **107**, 9628–9633.
34 J. P. Camden, H. A. Bechtel, D. J. Ankeny Brown, A. E. Pomerantz, R. N. Zare and R. J. Le Roy, *J. Phys. Chem. A*, 2004, **108**, 7806–7813.
35 A. B. Alekseyev, H.-P. Liebermann, D. B. Kokh and R. J. Buenker, *J. Chem. Phys.*, 2000, **113**, 6174–6185.
36 A. B. Alekseyev, D. B. Kokh and R. J. Buenker, *J. Phys. Chem. A*, 2005, **109**, 3094–3096.
37 J. A. Coxon and P. G. Hajigeorgiou, *J. Mol. Spectrosc.*, 1991, **150**, 1–27.
38 M. D. Feit and J. A. Fleck, *J. Chem. Phys.*, 1983, **78**, 301–308.
39 N. Balakrishnan, C. Kalyanaraman and N. Sathyamurthy, *Phys. Rep.*, 1997, **280**, 79–144.
40 B. Friedrich, personal communication.

